2013-04-15

Relationship between air-sea density flux and isopycnal meridional overturning circulation in a warming climate

Han, MyeongHee; Kamenkovich, Igor; Radko, Timour; Johns, William E.

Journal of Climate, Vol. 26, American Meteorological Society, 2013
http://hdl.handle.net/10945/42114

Relationship between Air–Sea Density Flux and Isopycnal Meridional Overturning Circulation in a Warming Climate

MYEONGHEE HAN AND IGOR KAMENKOVICH

Division of Meteorology and Physical Oceanography, Rosenstiel School of Marine and Atmospheric Science, University of Miami, Miami, Florida

TIMOUR RADKO

Department of Oceanography, Naval Postgraduate School, Monterey, California

WILLIAM E. JOHNS

Division of Meteorology and Physical Oceanography, Rosenstiel School of Marine and Atmospheric Science, University of Miami, Miami, Florida

(Manuscript received 15 November 2011, in final form 15 October 2012)

ABSTRACT

This study aims to explore the relationship between air–sea density flux and isopycnal meridional overturning circulation (MOC), using the Intergovernmental Panel on Climate Change (IPCC) Fourth Assessment Report (AR4) model projections of the twenty-first-century climate. The focus is on the semiadiabatic component of MOC beneath the mixed layer; this component is described using the concept of the push–pull mode, which represents the combined effects of the adiabatic push into the deep ocean in the Northern Hemisphere and the pull out of the deep ocean in the Southern Hemisphere. The analysis based on the GFDL Climate Model version 2.1 (CM2.1) simulation demonstrates that the push–pull mode and the actual isopycnal MOC at the equator evolve similarly in the deep layers, with their maximum transports decreasing by 4–5 Sv (1 Sv $\equiv 10^6$ m^3 s^{-1}) during years 2001–2100. In particular, the push–pull mode and actual isopycnal MOC are within approximately 10% of each other at the density layers heavier than 27.55 kg m^{-3}, where the reduction in the MOC strength is the strongest. The decrease in the push–pull mode is caused by the direct contribution of the anomalous heat, rather than freshwater, surface fluxes. The agreement between the deep push–pull mode and MOC in the values of linear trend and variability on time scales longer than a decade suggests a largely adiabatic pole-to-pole mechanism for these changes. The robustness of the main conclusions is further explored in additional model simulations.

1. Introduction

The climate of the earth is strongly affected by the ocean circulation, which carries a massive amount of heat from the tropics to the poles and from pole to pole (Talley et al. 2003; Boccaletti et al. 2005). In particular, the meridional overturning circulation (MOC), defined as a zonally integrated meridional flow in the ocean, plays an important role in the earth's climate (e.g., Stouffer et al. 2006). Understanding dynamics of the MOC is crucial for its prediction as the sea surface temperature increases in the twenty-first century (Clark et al. 2002). However, the mechanisms of MOC variability and its response to the climate change remain largely unclear. Lack of understanding of MOC dynamics complicates its accurate representation in climate models and contributes to significant uncertainty in climate model projections of the future MOC states. In particular, the sensitivity of the Atlantic MOC to surface forcing varies significantly from model to model (Gregory et al. 2005; Stouffer et al. 2006). Although most of the climate simulations reported by the Intergovernmental Panel on Climate Change (IPCC) show that the Atlantic MOC will slow down in the twenty-first

Corresponding author address: Igor Kamenkovich, Division of Meteorology and Physical Oceanography, Rosenstiel School of Marine and Atmospheric Science, University of Miami, 4600 Rickenbacker Causeway, Miami, FL 33149.
E-mail: ikamenkovich@rsmas.miami.edu

DOI: 10.1175/JCLI-D-11-00682.1

century, the magnitudes of the reduction vary significantly among the models (Meehl et al. 2007).

The dynamical causes of the weakening MOC in a warming climate are still under debate. Although the reduction in the surface density is expected to weaken deep convection in the high-latitude North Atlantic, the relation between the convection strength and intensity of deep water formation remains unclear (Marotzke and Scott 1999). Numerical simulations suggest a critical importance of the meridional density contrast (e.g., Wiebe and Weaver 1999; Klinger and Marotzke 1999; Marotzke and Klinger 2000), but the dynamics behind this relation are also under debate. Numerical studies also disagree in identifying the dominant components of the surface buoyancy fluxes. Some models demonstrate the importance of the increase in the freshwater input at high latitudes (Manabe and Stouffer 1994; Dixon et al. 1999; Schmittner and Stocker 1999; Wiebe and Weaver 1999), while others show the primary importance of heat flux anomalies (Mikolajewicz and Voss 2000; Kamenkovich et al. 2003). Factors other than surface forcing in the high-latitude North Atlantic may also play a significant role, including a stabilizing effect of the anomalous atmospheric moisture flux from the tropical Atlantic (Latif et al. 2000), or the stratification in the Southern Ocean (Kamenkovich and Radko 2011).

The fundamental connection between the surface buoyancy input and water movement, on the other hand, comes from the considerations of temperature and density balances. In particular, Walin (1982) found that the thermal circulation between the tropics and the pole is related to the thermal forcing at the ocean surface and proposed an elegant approach to relate the water mass transformation rates on isopycnal surfaces to the air–sea buoyancy fluxes. This approach has been utilized in a number of studies (Speer and Tziperman 1992; Speer et al. 1995; Marshall et al. 1999; Tandon and Zahariev 2001; Donners et al. 2005; Downes et al. 2011). In particular, Grist et al. (2009), using preindustrial control simulations with three IPCC models, found the maximum value of the MOC at 48°N to have a significant relationship with the surface-forced streamfunction in the North Atlantic.

Below the mixed layer, one can identify two main driving mechanisms of the MOC. In one mode, the MOC is controlled by diabatic mixing, resulting in cross-isopycnal motions (i.e., upwelling). The importance of this mechanism is manifested in strong sensitivity of the MOC to diapycnal mixing in numerical simulations (e.g., Bryan 1987). In the second, semiadiabatic mode, the water is moving along isopycnals, forced by mass exchanges with the mixed layer above; the cross-isopycnal fluxes below the mixed layer are neglected. A number of studies describe the significance of the resulting pole-to-pole branch of the MOC, for which the processes in the Southern Ocean are particularly important (Toggweiler and Samuels 1998; Gnanadesikan 1999; Samelson 2004, 2009; Wolfe and Cessi 2010; Radko and Kamenkovich 2011; Sévellec and Fedorov 2011).

A precise separation of the MOC into adiabatic and diabatic components is challenging, if not impossible. However, following the ideas of Walin (1982), one can attempt to estimate a portion of the MOC within a given basin (e.g., Atlantic) from the surface density fluxes and density, as well as lateral exchanges with other basins. This is the so-called ''push–pull mode'' whose meridional volume transport in the deep Atlantic ocean is driven by the isopycnal pull in the Southern Ocean and the isopycnal push from the north (Radko et al. 2008). This mode owes its existence to the interhemispheric asymmetry in the surface buoyancy input and represents the pole-to-pole component of the MOC that is adiabatic below the mixed layer (semiadiabatic). The relative importance of the push–pull mode can serve as a measure of the significance of the adiabatic dynamics of the MOC. In particular, Radko et al. (2008) concluded, using the output of a coarse-resolution numerical model, that approximately two-thirds of the MOC can be driven by semiadiabatic processes; see also Gnanadesikan (1999) for a similar conclusion. The share of the adiabatic component is likely to be even larger in nature, since the coarse-resolution numerical simulations of this type tend to have relatively high values of diapycnal diffusivity, both explicit and numerical, which are not supported by direct observational estimates (Ledwell et al. 1993; Toole et al. 1994).

The main objectives of this study are to describe changes in the pole-to-pole semiadiabatic MOC, using the concept of the push–pull mode, and examine processes that cause these changes. In particular, comparison of the variations in the actual isopycnal MOC with those in the push–pull mode will help to investigate if a significant portion of the total MOC changes can be attributed to the semiadiabatic push–pull mechanism on various time scales. More specifically, we will examine the relative importance of heat and freshwater fluxes in causing changes in the MOC (section 3.2) and compare the long-term trends (section 3.3) and interannual and interdecadal variability (section 3.4) between the push–pull mode and actual isopycnal MOC. The bulk of the analysis is carried out for the simulations of the Atlantic MOC using a GFDL model (section 3); simulations of the global MOC (section 4) and Atlantic MOC using three other IPCC models (section 5) will also be discussed.

2. Methodology and data

The methodology for calculating the semiadiabatic mode of circulation, the push–pull mode, is adapted from Radko et al. (2008); only a brief description is given here. Air–sea density flux (D) into the ocean is calculated using surface temperature, salinity, and heat and freshwater fluxes and is defined as below (Schmitt et al. 1989):

$$D = -\frac{\alpha H}{C_p} + \rho\beta\frac{1000(E-P-R)S}{1000-S}, \tag{1}$$

$$\alpha = -\frac{1}{\rho}\frac{\partial\rho}{\partial T}, \quad \beta = \frac{1}{\rho}\frac{\partial\rho}{\partial S}, \quad E = \frac{Q_{\text{lat}}}{L}, \tag{2}$$

where D is the air–sea mass flux in to the ocean (kg m^{-2} s^{-1}), α is the thermal expansion coefficient (positive), β is the haline contraction coefficient (positive), C_p is the specific heat capacity of water, E and P are the rates of evaporation and precipitation, H is the heat flux into the ocean, L is the latent heat of vaporization (2.5×10^6 J kg^{-1}), ρ is the density, Q_{lat} is the surface latent heat flux, R is the runoff, S is the salinity (psu), and T is the temperature. All calculations are carried out in density space, using potential density ρ_{pot} referenced to the surface. For convenience, we use the potential density anomaly σ, $\sigma = \rho_{\text{pot}} - 1000$ kg m^{-3}, and carry out the analysis in the density range from 1022.00 to 1028.00 kg m^{-3}.

The push–pull mode is calculated from the actual isopycnal overturning and volume exchanges between the mixed layer and oceanic interior. The isopycnal streamfunction is calculated using the vertical integration of the meridional volume transport from the bottom[1]:

$$\Psi(y,\sigma) = \int_{x_w}^{x_e} dx \int_{-H}^{Z(x,y,\sigma)} v\, dz, \tag{3}$$

where v is the Eulerian meridional velocity (the parameterized eddy-induced velocities are not added), Z is the height of the isopycnal surface σ, H is the depth of the ocean, x_e is the longitudinal easternmost point, and x_w is the longitudinal westernmost point.

The subducted volume transport at the bottom of the mixed layer can be diagnosed from the air–sea density flux D using the conservation of isopycnal volume within the mixed layer; see Radko et al. (2008) for a detailed derivation. The contribution of the diabatic eddies to this balance is neglected in the mixed layer, since these affects are assumed to be small[2] in comparison to the direct air–sea density flux term. Although this assumption is consistent with the scaling arguments in Radko (2007), the neglect of the diabatic eddy terms in this non-eddy-resolving model may introduce an additional source of disagreement between the push–pull mode and actual MOC.

The high-latitude regions present a challenge for several reasons. First, these regions are characterized by a deep and strongly seasonally varying mixed layer, for which the integrated effect of the diabatic processes, not accounted for by the push–pull mode approach, can be important. In particular, water mass conversions in the GCM-simulated Southern Ocean can be very significant (Downes et al. 2011). Second, the lack of meridional boundaries in the Atlantic section of the Southern Ocean (south of approximately 30°S) significantly complicates the calculation of the push–pull mode (Radko et al. 2008). Last, the presence of sea ice in high latitudes presents additional challenges for the analysis, since the ice–ocean heat/freshwater fluxes for these simulations are not available from the archived numerical model output.

To minimize these problems at high latitudes, the push–pull mode is calculated from the sea surface flux and density not over all latitudes, but for the region between 30°S and 65°N in the Atlantic; an alternative choice of 50°N for the northern boundary is also briefly considered below. Below the mixed layer, the volume divergence in each isopycnal layer in the Southern (Northern) Hemisphere, denoted by subscript n (s) below, is determined by the three groups of terms (Fig. 1): the lateral volume transports across the equator and 30°S (65°N), volume exchanges with the mixed layer, and diapycnal fluxes. The push–pull mode from 30°S to 65°N can then be defined [see Radko et al. (2008), Han (2011), and the appendix]:

$$\text{PP}^{65}(\sigma) = \frac{1}{2}[B_s - B_n]_{\sigma_{\max}}^{\sigma} + \frac{1}{2}(\Psi_a^{30\text{S}} + \Psi_a^{65\text{N}}), \tag{4}$$

where $\Psi_a^{30\text{S}}$ and $\Psi_a^{65\text{N}}$ are the isopycnal streamfunctions (3) at 30°S and 65°N, respectively, in the Atlantic; $[f]_{\sigma_1}^{\sigma_2} = f(\sigma_2) - f(\sigma_1)$; and

$$B_{s,n}(\sigma) = \lim_{\Delta\sigma\to 0}\frac{1}{\Delta\sigma}\iint D(x,y)\, dx\, dy, \tag{5}$$

[1] For simplicity, the smallest isopycnal depth is chosen in situations when the potential density is double valued.

[2] This assumption does not, however, imply that these fluxes are too small to matter for other dynamical processes.

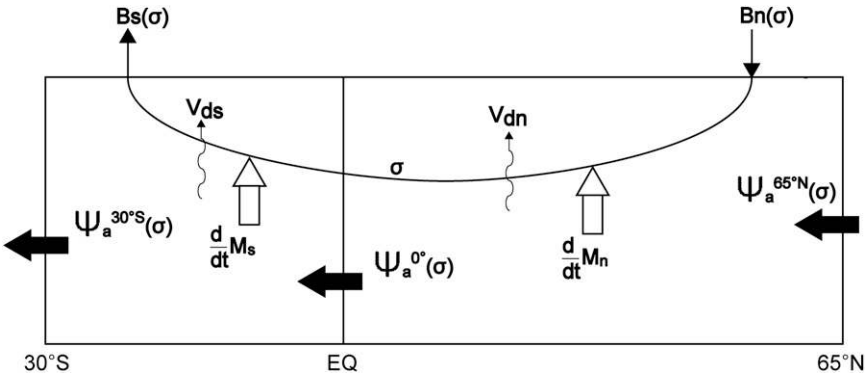

FIG. 1. The concept of the push–pull mode employed in this study. Arrows indicate various terms in (4) and (6) that control the volume below an isopycnal σ in each hemisphere.

which is known as the water mass transformation function (Walin 1982). The integral in (5) is taken over the surface area δA between σ and $\sigma + \Delta\sigma$. Equation (4) stands for the volume flux between an isopycnal σ and the bottom, which is directly forced (pushed/pulled) from the surface and lateral boundaries. It includes the surface push–pull mode (SPP_a) component attributed to surface density fluxes (first group of bracketed terms), as well as contributions from the lateral exchanges with the regions south and north of the analyzed region (second group of bracketed terms). The push–pull mode diagnosed in this way was shown to be closely connected to the actual isopycnal MOC at the equator by Radko et al. (2008).

However, in the presence of diapycnal mixing and changing isopycnal volumes, the connection between the push–pull mode and MOC is less direct. As discussed in the appendix, these two quantities are related as follows:

$$\Psi_a^0(\sigma) = \mathrm{PP}^{65}(\sigma) + \frac{1}{2}[V_{dn}(\sigma) - V_{ds}(\sigma)] + \frac{1}{2}\frac{d}{dt}[M_n(\sigma) - M_s(\sigma)], \quad (6)$$

where $V_{d(n,s)}$ are the interior diapycnal fluxes through the isopycnal σ in the Northern (Southern) Hemisphere and $M_{n,s}$ are the volumes bounded from above by this isopycnal. Thus, the difference between the push–pull mode and the equatorial MOC could be substantial if either the diapycnal fluxes or the variability in the isopycnal volumes are large and exhibit significant intrahemispheric asymmetry. In this study, the 100-yr average of the third term in Eq. (6) (isopycnal volume drift) is demonstrated to be small (not shown): for the GFDL model, it is less than 1.5 Sv at its maximum at $\sigma = 27.85$ and less than 0.75 Sv at densities above $\sigma = 27.7$. The short-term changes can, however, be more significant.

All calculations are carried out for monthly values of density, velocity, and surface fluxes. This study is primarily focused on the global-change simulation carried out for the IPCC Fourth Assessment Report (AR4), using the Geophysical Fluid Dynamics Laboratory (GFDL) Climate Model version 2.1 (CM2.1) (Griffies et al. 2005). Outputs from three other IPCC models—the Canadian Centre for Climate Modeling and Analysis (CCCMA; Flato et al. 2000), the Model for Interdisciplinary Research on Climate (MIROC; Hasumi and Emori 2004), and the National Center for Atmospheric Research (NCAR; Smith and Gent 2004) climate models—are analyzed in order to assess the robustness of the main conclusions in the Atlantic Ocean. These simulations are not eddy resolving; the spatial resolutions are given in Table 1. All simulations adopt the Special Report on Emissions Scenarios (SRES) A2 scenario of greenhouse gas emissions, which contains the strongest greenhouse forcing for the future considered in the AR4 assessment (DDC IPCC 2010).

TABLE 1. Zonal, meridional, and vertical resolutions of GFDL, CCCMA, MIROC, and NCAR models (Flato et al. 2000; Griffies et al. 2005; Hasumi and Emori 2004; Smith and Gent 2004).

Models	Zonal resolution	Meridional resolution	Vertical resolution
GFDL	360 grids	200 grids	50 grids
	1°	1° (1/3°)	10–366 m
CCCMA	192 grids	96 grids	29 grids
	1.8750°	1.8559–2.2756°	50–300 m
MIROC	256 grids	192 grids	33 grids
	1.406 25°	0.56–1.40°	10–500 m
NCAR	395 grids	320 grids	40 grids
	1.125°	0.2671–0.5342°	10–250 m

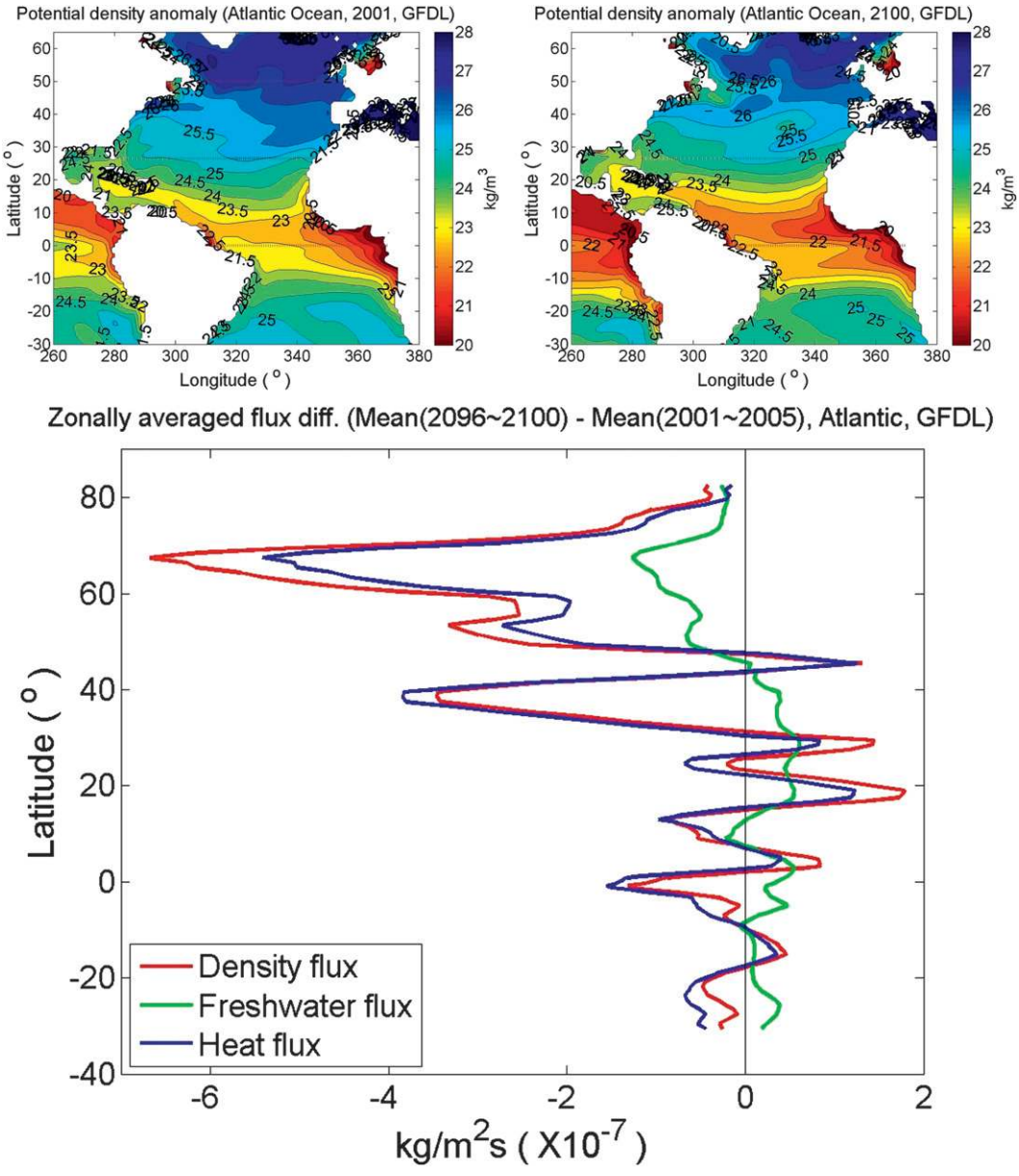

FIG. 2. Change in the air–sea density flux and its components. (top) The difference between the 2096–2100 and 2001–05 time averages of zonally averaged surface fluxes in the Atlantic Ocean [Eq. (1)] are shown here (bottom) as functions of latitude: density flux (red), freshwater part of density flux (green), and heat flux part of density flux (blue).

3. Atlantic MOC: GFDL model

The air–sea density flux D and sea surface density in the GFDL CM2.1 model both evolve during the years 2001–2100, with particularly significant changes in the North Atlantic. The differences in the density flux between the last 5-yr (2095–2100) and first 5-yr (2001–05) means in the Atlantic are shown in Fig. 2. As is indicated by the negative values around 65°N, there is a significant increase in the buoyancy input in the northern North Atlantic, resulting in the decreasing surface density in this region. These changes in the surface density fluxes can project strongly onto the push–pull mode. In contrast, there is no systematic change in the surface density input in the South Atlantic, north of 30°S.

These changes in the sea surface density and density fluxes lead to significant changes in the MOC in the Atlantic basin and globally during years 2001–2100. The isopycnal Atlantic MOC weakens substantially in the deep layers, with the most pronounced changes

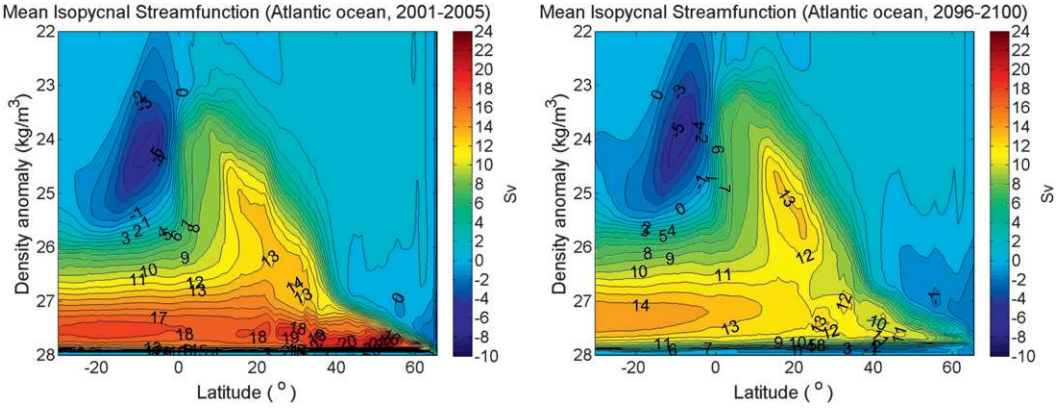

FIG. 3. Isopycnal MOC streamfunction averaged over (left) 2001–05 and (right) 2096–2100, shown from 30°S to 65°N as a function of density and latitude.

observed in the Northern Hemisphere. The maximum in the overturning shifts to lighter densities, resulting in a 6–20-Sv decrease at a given density surface (Fig. 3). In the following analysis, these changes will be examined and interpreted, using the concept of the push–pull mode.

Prior to the analysis of the push–pull mode and its changes with time, an appropriate choice of the northern boundary should be made. Two options for the northern boundary of the computational domain are considered here, one including (65°N) and one excluding (50°N) the high-latitude region 50°–65°N. The latter region is characterized by active convective sites and a deep mixed layer, both associated with the deep water formation in the North Atlantic; it also includes significant amounts of sea ice. The importance of the processes in the 50°–65°N region is briefly examined in this section.

To examine the importance of the sea ice for the push–pull mode, we compare the push–pull mode calculated from surface density fluxes with and without the surface fluxes in the ice-covered regions. Three options were considered, but led to nearly identical results. In the first settings, the density fluxes from/into the ocean are calculated as the fluxes into/from the atmosphere times the ice concentration. In the second setting, the density fluxes over the ice-covered regions are set to zero regardless of the ice concentration. In the third setting, the buoyancy fluxes under the ice are assumed to equal the fluxes on top of it. We conclude that the surface fluxes over ice-covered regions have a secondary importance for the push–pull mode dynamics. In the rest of the discussion, the push–pull mode is calculated with the sea ice effects ignored, as in the third method.

The push–pull modes calculated with the northern boundary set at 50°N (PP_a^{50}) and 65°N (PP_a^{65}) are similar throughout the analyzed 100-yr period (Fig. 4), and the rest of the analysis is primarily focused on PP_a^{65}; only brief comparison with PP_a^{50} is done where appropriate. The density corresponding to the maximum MOC ($\sigma_{\Psi\max}$) is, however, somewhat lighter in PP_a^{65} than in PP_a^{50}. This is plausibly related to the cross-isopycnal mixing with denser waters in the latitudes between 50° and 65°N, where most of the deep water formation takes place; the mixing acts to increase the density of the water that is being "pushed" from the surface. The surface push–pull mode and the actual isopycnal MOC at 30°S (Ψ_a^{30S}), consequently, are the main components of the push–pull mode; their relative importance is further examined in section 3.1.

As is argued by Radko et al. (2008) and in section 2, the difference between the push–pull mode and the actual isopycnal MOC is dependent on the distribution of

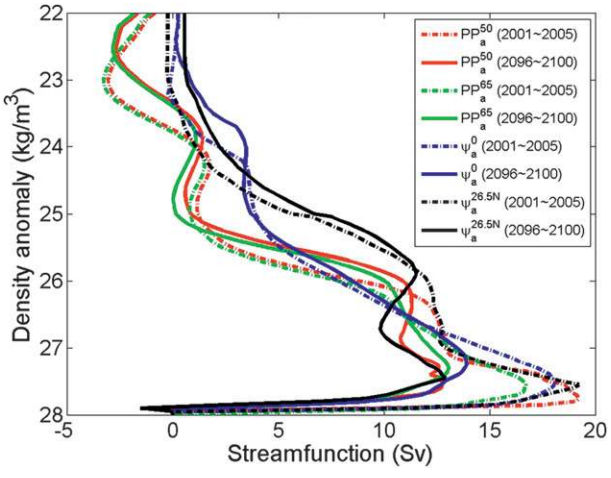

FIG. 4. Actual Atlantic MOC and the push–pull mode. The 2001–05 (dash–dotted lines) and 2096–2100 (solid lines) time averages of the PP_a^{50} (red), PP_a^{65} (green), Ψ_a^0 (blue), and Ψ_a^{26N} (black) are shown as functions of density in the Atlantic Ocean.

TABLE 2. Changes in the maximum transport and corresponding density of the push–pull mode and actual isopycnal MOC in the Atlantic Ocean.

	2001–05 mean		2096–2100 mean	
	Transport (Sv)	Density (kg m^{-3})	Transport (Sv)	Density (kg m^{-3})
PP_a^{50}	19.23	27.75	12.73	27.55
PP_a^{65}	16.71	27.55	13.05	27.30
Ψ_a^{30S}	18.05	27.55	15.00	27.35
Ψ_a^{0}	18.08	27.50	13.90	27.25
$\Psi_a^{26.5N}$	19.22	27.55	12.93	27.45
Ψ_a^{65N}	5.43	27.90	2.68	27.75

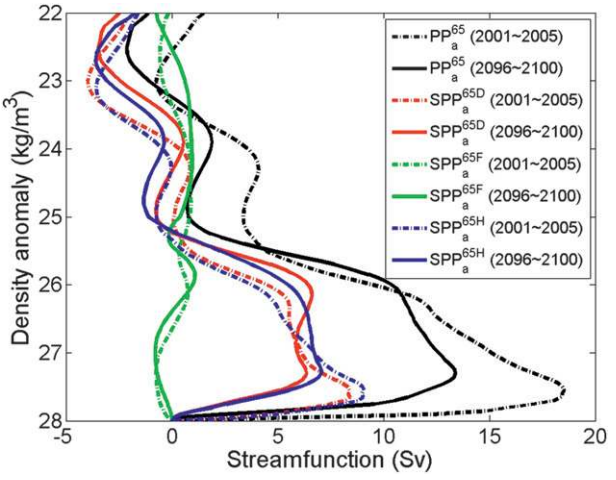

FIG. 5. Surface push–pull mode and its components in the Atlantic Ocean. The 2001–05 (dash–dotted lines) and 2096–2100 (solid lines) averages of the push–pull mode (30°S–65°N, black) and the surface push–pull mode (30°S–65°N), calculated from the density flux (red), freshwater flux part (green), and heat flux part (blue), are shown here as functions of density.

diapycnal mixing and isopycnal volume drifts and should be the smallest at the equator. This, however, assumes a roughly symmetric distribution of diabatic water mass transformation around the equator. To assess the importance of diapycnal flux distribution, we analyze the actual isopycnal MOC at two locations—the equator (Ψ_a^0) and 26.5°N ($\Psi_a^{26.5N}$)—and compare the results with the push–pull mode.

The push–pull mode and actual isopycnal MOC both weaken in response to the changing buoyancy forcing (Fig. 4). In particular, the 5-yr average of the maximum MOC decreases significantly during 100 years by 3.7 Sv (PP_a^{65}), 4.2 Sv (Ψ_a^0), and 6.3 Sv ($\Psi_a^{26.5N}$); $\sigma_{\Psi max}$ shifts to lighter densities (Table 2), which results in even bigger changes in the MOC at a given density. At the same density, for example, PP_a^{65} decreases by 5.0 Sv from 16.71 to 11.74 Sv at 27.55 kg m^{-3}.

The push–pull mode and actual isopycnal MOC at the equator are generally close to each other in the deep density layers. More specifically, PP_a^{65} and Ψ_a^0 are very similar at the densities heavier than 27.00 kg m^{-3}; the difference between PP_a^{65} and Ψ_a^0 is less than 1 Sv at the densities 25.90–26.85 kg m^{-3} during years 2001–05 and 27.25–27.55 and 27.85–28.00 kg m^{-3} during 2096–2100. The differences are larger for lighter densities but are still less than 2 Sv at densities heavier than approximately 25.70 kg m^{-3}. At the density heavier than 27.55 kg m^{-3}, where the largest MOC values are found, PP_a^{65} is 93% ± 5% (2001–05 average) and 89% ± 4% (2096–2100 average) of Ψ_a^0. In contrast, the differences are larger between the push–pull mode and Ψ_a^0 in the layers shallower than, approximately, 25.5 kg m^{-3}; see Radko et al. (2008) for a similar conclusion.

The differences between PP_a^{65} and actual overturning at 26.5°N are more significant, especially at years 2001–05 (Fig. 4). This indicates a stronger asymmetry (relative to this latitude) in the spatial distribution of diapycnal fluxes and isopycnal volume drifts. The asymmetric distribution of diapycnal fluxes can be seen in Fig. 3, which shows that most of the water mass transformation from light to dense waters takes place north of 26.5°N. Nevertheless, although $\Psi_a^{26.5N}$ is substantially stronger than PP_a^{65} (by 3–4 Sv), the overall pattern of MOC and the value of $\sigma_{\Psi max}$ are similar.

a. Surface and lateral boundary components

The push–pull mode PP_a^{65} is a combination of the surface and ''lateral boundary'' components. As discussed in section 2, the surface component quantifies the contribution of air–sea buoyancy exchanges, whereas the lateral boundary component, since it is dominated by Ψ_a^{30S}, mainly describes the influence of the Southern Ocean. The push–pull formalism allows direct examination of the relative importance of each of these components.

To examine the direct contribution of the air–sea density flux into the ocean, the surface push–pull component (SPP_a^{65D}) is analyzed here separately from the full push–pull mode (Fig. 5). The value SPP_a^{65D} weakens significantly at densities heavier than 27.00 kg m^{-3} during years 2001–2100, which influences the reduction in the total push–pull mode and shifts $\sigma_{\Psi max}$ to lighter values. In particular, the maximum of the 5-yr average of SPP_a^{65D} decreases by more than 2 Sv, changing from 8.40 Sv at 27.65 kg m^{-3} to 6.35 Sv at 27.30 kg m^{-3}. This decrease in SPP_a^{65D} is driven primarily by changes in the high-latitude fluxes of the North Atlantic.

The freshwater and heat flux components in (1) are next used to calculate their direct individual contributions to the surface push–pull mode. It is important to

emphasize that this straightforward analysis cannot accurately isolate the importance of freshwater fluxes for the MOC weakening, since these fluxes can have a strong indirect influence on the surface heat gain/loss through changes in circulation. The first 5-yr and last 5-yr means of the resulting surface push–pull modes are shown in Fig. 5 as functions of density. The surface push–pull modes calculated from the full density flux (SPP_a^{65D}) and heat flux only (SPP_a^{65H}) are very close at all density layers; the maximum of SPP_a^{65H} decreases from 9.07 Sv (at 27.55 kg m^{-3}) to 7.06 Sv (at 27.25 kg m^{-3}). The freshwater (SPP_a^{65F}) contribution is, in contrast, significantly smaller. We conclude that the surface push–pull mode is dominated by the contribution from the heat flux, rather than the freshwater flux.

The role of the lateral boundary components can be readily estimated by the difference between PP_a^{65} and SPP_a^{65D} (black and red lines in Fig. 5). This lateral boundary component is dominated by the isopycnal flow across 30°S, since the MOC at 65°N is small. The component is at least as large as the surface push–pull mode at both 2001–05 and 2096–2100 periods. This result signifies the importance of the Southern Ocean in MOC and will be further explored and interpreted in section 5 for additional model simulations.

b. Linear trends in MOC

The maximum isopycnal MOC and push–pull modes exhibit similar and nearly linear downward trends in time at densities heavier than 27.00 kg m^{-3} (Fig. 6, top). Note that the values of these maxima do not correspond to the same density values. Most significantly, the linear trends in the maximum PP_a^{65} and Ψ_a^0 are very similar to each other, -0.047 Sv yr^{-1} and -0.040 Sv yr^{-1}, respectively. The values of maximum $\Psi_a^{26.5N}$ are larger than in PP_a^{65} (see also Fig. 3). Interestingly, PP_a^{50} exhibits the strongest downward linear trend (-0.063 Sv yr^{-1}) among all measure of MOC.

The rate of change in the MOC is further quantified in Fig. 6 (bottom) using the linear trends computed for each density and absolute values of the corresponding streamfunctions. All measures of MOC exhibit a negative linear trend for the densities greater than 26.80 kg m^{-3}, and the largest negative linear trends in PP_a^{65}, Ψ_a^0, and $\Psi_a^{26.5N}$ are observed at the densities higher than 27.80 kg m^{-3}. In contrast, the linear trends of the push–pull mode are larger than the actual MOC at the densities higher than 27.70 kg m^{-3}.

The difference in the linear trends between Ψ_a^0 and the push–pull mode is in large part because of the interhemispheric asymmetry in the MOC changes. Given the smallness of the isopycnal volume drifts, this asymmetry is primarily linked to the diapycnal fluxes and related

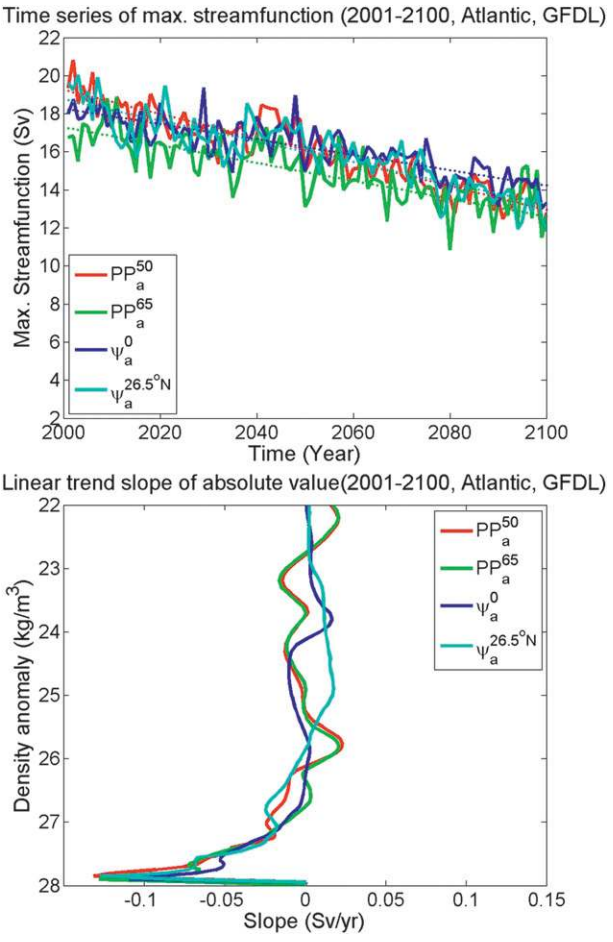

FIG. 6. Interannual variability and linear trends in the Atlantic MOC. Shown are (top) the time series and the fitted linear trends of the maximum and (bottom) the slope of the linear trend (Sv yr^{-1}) as functions of density for PP_a^{50} (red), PP_a^{65} (green), Ψ_a^0 (blue), and $\Psi_a^{26.5N}$ (cyan).

upwelling since, in the absence of these processes, the isopycnal MOC would weaken uniformly at all latitudes. In particular, changes in the Northern Hemispheric MOC are significantly larger than in the Southern Hemisphere (Table 2), indicating significant changes in the North Hemisphere upwelling and in the interhemispheric distribution of the diapycnal fluxes. This issue will be further investigated in section 5.

c. Interannual and interdecadal variability

The variability in the MOC at time scales from one year to a decade can be expected to be more challenging to capture and interpret using the push–pull mode. This is mainly because the adjustment of the pole-to-pole MOC can take several years, and the drifts in the isopycnal volumes [third group of terms in Eq. (6)] are likely to be more significant. The analysis of this section

explores the limits to which the push–pull mode can be used to interpret changes in the actual isopycnal MOC. We begin with variability on scales longer than one year. We loosely define this variability as ''interannual'', although it also involves decadal time scales, and demonstrate that the correlation between MOC and the push–pull mode on these scales is modest, but statistically significant. The correlation at the decadal time scales is, in contrast, demonstrated to be very strong.

To examine the relationship between the annual anomalies in the push–pull mode and actual isopycnal MOC among different density layers, the cross-correlation coefficients (for all pairs of densities) among values of the push–pull mode, Ψ_a^0, and $\Psi_a^{26.5N}$ are calculated. These values are shown in Fig. 7 at zero time lag, and the linear trend is removed from the time series. The correlations between the push–pull mode and Ψ_a^0 exceed 0.35 in the deep and intermediate layers, where the push–pull mode also tends to be best correlated with Ψ_a^0 at slightly lighter densities. In contrast, correlation between the push–pull mode and actual MOC is lacking at 25.8–26.7 kg m^{-3}. This density range includes the intergyre boundary of the North Atlantic at the surface (Fig. 2, top) and is also characterized by transformations within the subtropical gyre (Fig. 3); it is, therefore, probable that diapycnal fluxes and variability in isopycnal volumes can be significant enough to break down the correlation. The correlation of 0.3 at even lighter densities of 25.4–25.6 kg m^{-3} is then somewhat puzzling and might be a consequence of mutually compensating fluctuations in isopycnal volumes.

The relationship between the annual anomalies in the push–pull mode and $\Psi_a^0/\Psi_a^{26.5N}$ for different time lags and the same density is analyzed next (Fig. 8, top). Positive time-lag values correspond to PP_a^{65}, lagging the actual MOC. Note that the analysis at the same density can underestimate the correlation between the isopycnal MOC and push–pull mode because of the importance of diapycnal processes. For example, a volume anomaly pushed into an isopycnal layer can later ''leak'' into a different isopycnal layer because of diapycnal exchanges. Such processes can explain density biases between the push–pull mode and actual MOC in Figs. 4, 7. To account for these effects, we calculated correlations among all pairs of densities for each given time lag; the density biases are not, however, found to be significant in the deep layers.

The correlation coefficients exceed 0.3 for several time lags and vary among difference densities. In particular, PP_a^{65} leads Ψ_a^0 at the time lags of 6–7 yr at 27.9 kg m^{-3} and lags Ψ_a^0 at the time lags of 1 and 3–5 yr for most of other density values (Fig. 8, top left). The maximum correlation (among all densities) is 0.40 (zero lag). The correlations between the push–pull mode and $\Psi_a^{26.5N}$ tend to be higher, with the correlation coefficients exceeding 0.35 for negative lags (PP_a^{65} leading) of 5–6 yr and positive lags (PP_a^{65} lagging) of 2–6 yr (Fig. 8, top right). The maximum values (among all density pairs) are 0.51 for the time lags of −5 and 0.49 for the time lags of 2 yr. All these values correspond to deep layers ($\sigma >$ 27.8 kg m^{-3}). Additionally, a correlation of 0.4 is also found at a time lag of 2 yr between PP_a^{65} and Ψ_a^0 at the intermediate water densities of $\sigma >$ 27.45 kg m^{-3}.

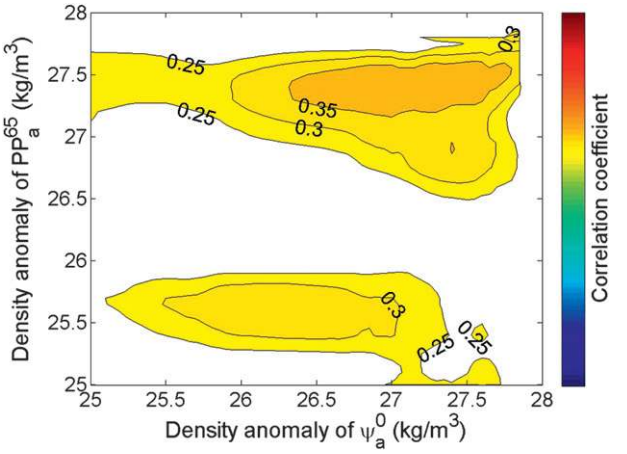

FIG. 7. Correlation between annual MOC anomalies at zero time lag. Shown are the cross-correlation coefficients between all density pairs for the push–pull modes (PP_a^{65}) and actual isopycnal MOC (Ψ_a^0) in the Atlantic Ocean (5% significance level).

How well can the push–pull mode capture the interdecadal variability? To address this question and understand the relationship between the decadal anomalies in the push–pull mode and the actual isopycnal MOC, the cross-correlation coefficients are computed for the low-pass filtered (by the 11-yr moving average) values of the push–pull mode and $\Psi_a^0/\Psi_a^{26.5N}$. The resulting correlation coefficients (Fig. 8, bottom) are substantially higher than in the full (unfiltered) time series. In particular, the maximum correlations between PP_a^{65} and actual isopycnal MOC (Ψ_a^0 and $\Psi_a^{26.5N}$) are above 0.5 for a wide range of time lags shorter than 10 yr. In the deep-to-intermediate layers, the highest correlations (>0.8) are found at short-time lags (0–5 yr). For Ψ_a^0, in particular, the maximum correlations are in the intermediate-to-deep layers (27.4–27.65 kg m^{-3}) and at zero time lag. The similarity of these maxima in Fig. 8 (left) suggests that the correlation between the decadal anomalies can, in large part, explain a correlation between the annual anomalies in the push–pull mode and actual MOC. Additionally, strong correlations at the negative lags of 3–7 yr (PP_a^{65} leading) are found at the intermediate levels (27.0–27.2 kg m^{-3}).

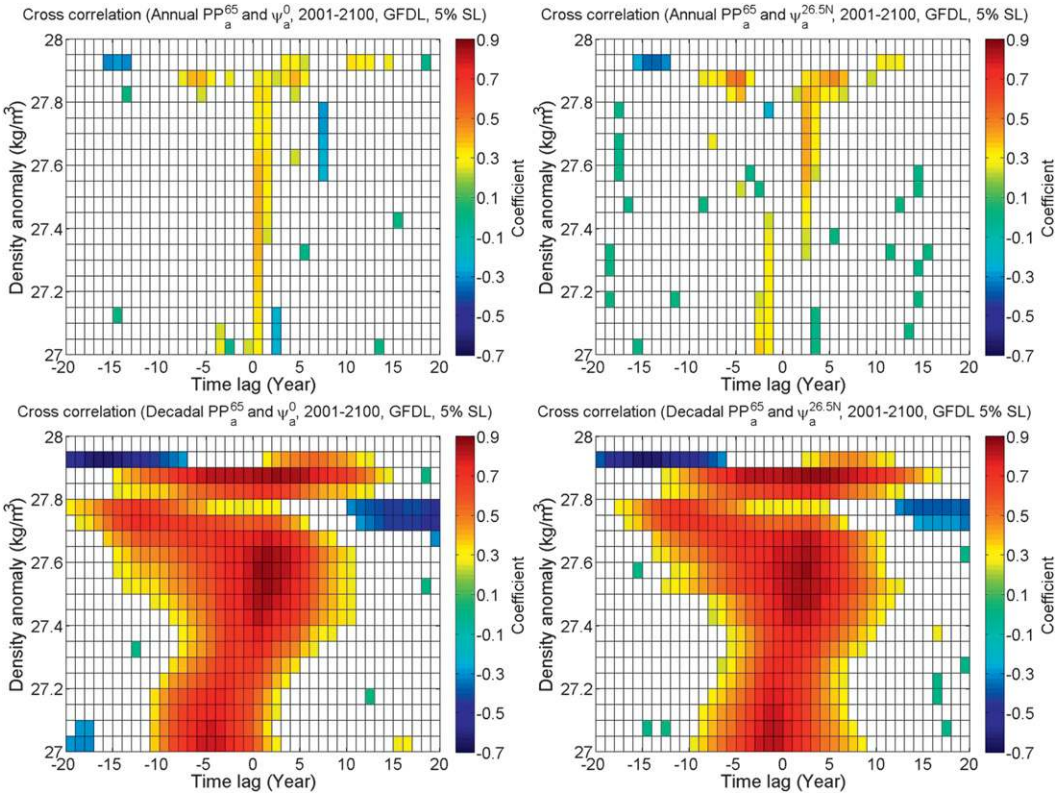

FIG. 8. Correlation between the (top) annual and (bottom) decadal MOC anomalies for various time lags. The cross-correlation coefficients for the same density are shown as functions of time lags between −20 and 20 yr for densities greater than 27.0 kg m^{-3} and for (left) PP_a^{65} and Ψ_a^0 and (right) PP_a^{65} and $\Psi_a^{26.5N}$. Positive time-lag values correspond to PP_a^{65} leading the actual MOC; values below 5% significance level are left blank.

The interpretation of the sign of these time-lag values is not straightforward, as the variability in the deep push–pull mode is affected by the two sources, the Southern Ocean (Ψ_a^{30S}) and the North Atlantic [high-latitude B_n, which dominates SPP_a in Eq. (4)]. In particular, one can expect the North Atlantic thermohaline forcing to lead the Northern Hemisphere MOC (Grist et al. 2009); the negative time-lag values in Fig. 8 may, therefore, be explained by this mechanism. In contrast, the Southern Hemisphere MOC can be expected to lag the overturning in the Northern Hemisphere, and our analysis indeed shows that Ψ_a^{30S} leads Ψ_a^0 and $\Psi_a^{26.5N}$. Alternative interpretations of positive time lags in Fig. 8 are also possible. In particular, Mahajan et al. (2011) demonstrate, in the same model, that the low-pass filtered Atlantic multidecadal oscillation (AMO) index lags Atlantic MOC (AMOC) variability by approximately 2 yr, which indicates the role of changes in circulation driving fluctuations in the surface heat flux.

The magnitude of the time lags can be explained by several physical processes, including fast propagation of Kelvin waves and slow propagation of baroclinic Rossby waves, as well as advection within the deep western boundary currents. In particular, short-term correlations (0–2 yr) between $\Psi_a^0/\Psi_a^{26.5N}$ and Ψ_a^{30S}/high-latitude B_n can only be explained by the Kelvin wave mechanism (e.g., Kawase 1987; Goodman 2001; Ivchenko et al. 2004). Time lags of 5–6 yr are, in contrast, broadly consistent with the advective mechanism (Zhang 2008) and, possibly, Rossby wave propagation. The latitude where the MOC is calculated (0° or 26.5°N) is also likely to be important. In particular, the fact that PP_a^{65} leads Ψ_a^0 on longer time scales than it leads $\Psi_a^{26.5N}$ (negative lags at σ = 27.0–27.2 kg m^{-3}) is likely to be a consequence of the relative proximity of 26.5°N to the high-latitude North Atlantic.

4. Global MOC: GFDL model

The analysis of the previous section is extended here to the global domain. The definitions of the actual isopycnal MOC and push–pull mode are otherwise the same as in the Atlantic basin, and the push–pull mode is computed between 30°S and 65°N. Exclusion of the Southern Ocean from this calculation removes the impact of diapycnal fluxes and significant water mass transformations in the Southern Ocean (Radko et al.

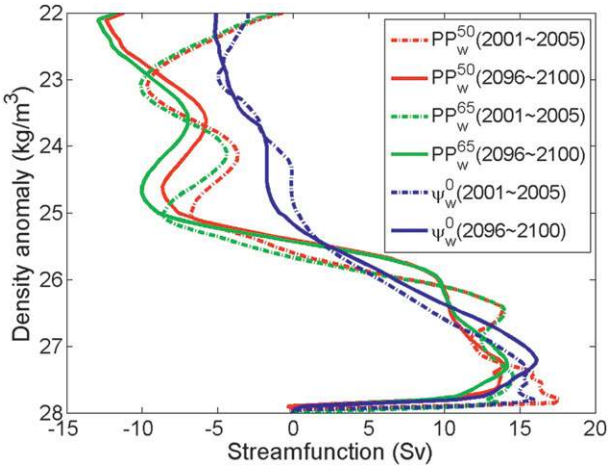

FIG. 9. Push–pull mode and actual equatorial MOC in the global ocean. The 2001–05 (dash–dotted lines) and 2096–2100 (solid lines) averages of PP_w^{50} (red), PP_w^{65} (green), and Ψ_w^0 (blue) are shown here as functions of density.

2008; Downes et al. 2011) and simplifies the comparison with the Atlantic-only results of the previous section. Additionally, limiting the domain to the one north of 30°S eliminates the direct influence of buoyancy exchanges underneath the sea ice in this study.

As in the Atlantic basin, the MOC changes significantly during the 100-yr period (Fig. 9). In particular, $\sigma_{\Psi\max}$ shifts from the deep (27.80 kg m^{-3}) to intermediate (27.20 kg m^{-3}) densities (Table 3); this shift is larger than in the Atlantic basin, where the maximum MOC is initially (years 2001–05) shallower. The maximum magnitude of Ψ_w^0, however, remains nearly the same. This is partly due to a smaller 2001–05 value in the global MOC in comparison with the Atlantic one, explained by a partial compensation between the southward-flowing deep water in the Atlantic and the northward-flowing deep water in the Indo-Pacific basin. The depth and strength of maximum Ψ_w^0 at years 2096–2100 are, in contrast, very similar to Ψ_a^0 (the magnitude is only 2.2 Sv larger in the global one).

Qualitatively similar changes are observed in the push–pull mode, with weakening in the maximum PP_w^{65} of only 0.5 Sv, and a shift of $\sigma_{\Psi\max}$ to lighter densities (also similar to PP_a^{65}). Interestingly, these changes cannot be attributed to Ψ_w^{30} since it intensifies with time (by 2 Sv total) and does not significantly change its position in the density space (27.2–27.25 kg m^{-3}). The linear trend in the maximum PP_w^{65} is very similar to that in Ψ_w^0, −0.032 and −0.032 Sv yr^{-1}, respectively. The linear trends in PP_w^{50} and PP_w^{65} are nearly identical in the upper ocean but are different in the deep layers.

Although the evolutions of the maximum PP_w^{65} and Ψ_w^0 are qualitatively similar (Fig. 10, top), the linear trend in

TABLE 3. Changes in the maximum transport and corresponding density of the push–pull mode and actual isopycnal MOC in the global domain.

	2001–05 mean		2096–2100 mean	
	Transport (Sv)	Density (kg m^{-3})	Transport (Sv)	Density (kg m^{-3})
PP_w^{50}	17.61	27.80	13.91	27.30
PP_w^{65}	14.56	27.50	14.15	27.30
Ψ_w^{30S}	16.07	27.25	18.04	27.20
Ψ_w^0	15.96	27.80	16.11	27.20
Ψ_w^{65N}	5.33	27.90	2.45	27.75

the maximum PP_w^{65} (−0.037 Sv yr^{-1}) is steeper than in Ψ_w^0 (−0.032 Sv yr^{-1}). Overall, the differences between the linear trends in PP_w^{65} and Ψ_w^0 are larger than those in the Atlantic basin (bottom panels of Figs. 6, 10). This fact indicates a substantial disagreement between the actual MOC and push–pull mode in the Indo-Pacific basin, most likely explained by the importance of

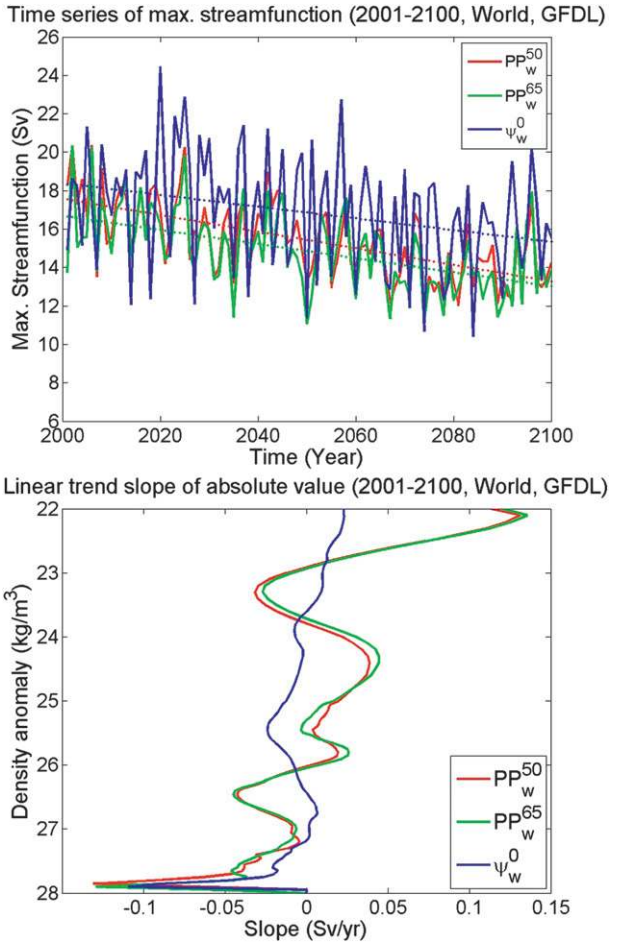

FIG. 10. Interannual variability and linear trends in the global MOC. Shown are (top) the time series and the fitted linear trends of the maximum and (bottom) the slope of the linear trend (Sv yr^{-1}) as functions of density for PP_w^{50} (red), PP_w^{65} (green), and Ψ_w^0 (blue).

diapycnal fluxes. This result is in a good agreement with Radko et al. (2008), who arrived at a similar conclusion using an ocean-only model in a steady state. The linear trends in PP_w^{50} and PP_w^{65} are nearly identical in the upper ocean but are different in the deep layers (Fig. 10, bottom).

5. Atlantic MOC in an ensemble of climate models

The push–pull modes and actual isopycnal MOC are analyzed here for three additional climate models: CCCMA, MIROC, and NCAR. The analyses of these very different simulations help to assess the robustness of the main conclusions and further interpret the differences between the semiadiabatic push–pull mode and the actual MOC. Not surprisingly, the differences in Ψ_a^0 between these simulations are substantial. The volume transport of the actual MOC varies significantly among simulations, ranging from 3–8 Sv in the CCCMA to 13–19 Sv in the NCAR simulations (Fig. 11). Anomalous buoyancy forcing leads to weakening of Ψ_a^0, but the simulations also differ in the magnitude of these changes (Table 4).

In all simulations, the maximum transports in the actual equatorial MOC are close to at least one of the push–pull modes (PP_a^{65} or PP_a^{50}). As in the GFDL model, two push–pull modes (PP_a^{65} and PP_a^{50}) are close to each other in the CCCMA simulation. However, MIROC and NCAR simulations exhibit substantial differences between these two push–pull modes, with PP_a^{65} always being smaller than PP_a^{50}. By definition of the push–pull mode, these differences originate from the region between 50° and 65°N and can be caused by strong diapycnal mixing, isopycnal volume changes, and/or influence of sea ice in these two models. Excluding this region in the push–pull mode calculation typically decreases the difference between the equatorial MOC and the push–pull mode, and PP_a^{50} and Ψ_a^0 are close to each other in all simulations except the MIROC one. The value Ψ_a^0 in the latter simulation is also surprisingly weaker than Ψ_a^{30S}.

The downward linear trend in Ψ_a^0 is generally consistent with the push–pull mode, although some differences are noticeable. Interestingly, the difference between PP_a^{65} and Ψ_a^0 trends is closely linked to the interhemispheric asymmetry in the response of the MOC to atmospheric forcing, which can be generally expected from the formulation of the push–pull mode. In particular, the difference in the linear trends in the maximum PP_a^{65} and Ψ_a^0 increases with the ''asymmetry measure,'' defined as the difference in the linear trends in the maximum Ψ_a^{30S} and $\Psi_a^{26.5N}$. Interestingly, the GFDL simulation exhibits the largest asymmetry in the response among the entire group of models. The depth of the maximum linear trend is also captured correctly by the push–pull modes in all models except CCCMA, where this maximum is

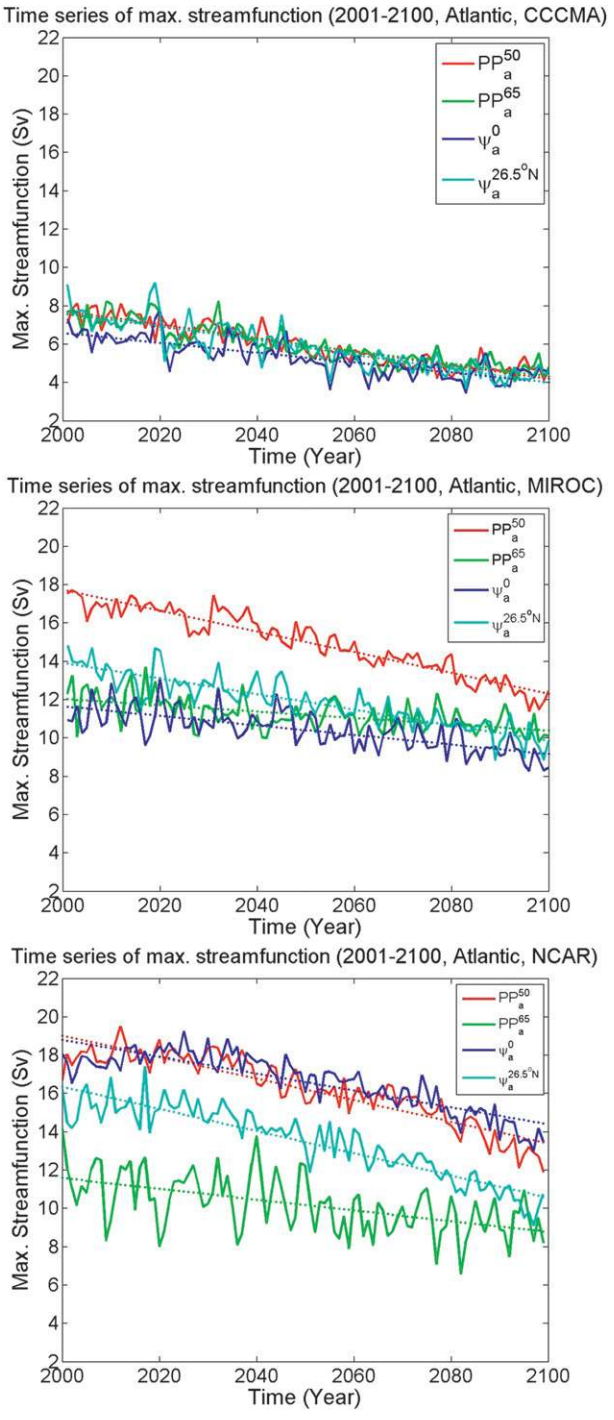

FIG. 11. Interannual variability and linear trends in the Atlantic MOC in three IPCC models: (top) CCCMA, (middle) MIROC, and (bottom) NCAR. Shown are the time series and the fitted linear trends of the maximum for PP_a^{50} (red), PP_a^{65} (green), Ψ_a^0 (blue), and $\Psi_a^{26.5N}$ (cyan).

TABLE 4. Linear trends of maximum PP_a^{50}, PP_a^{65}, Ψ_a^{30S}, Ψ_a^{0}, $\Psi_a^{26.5N}$, and Ψ_a^{65N} (Sv yr^{-1}) in the Atlantic during 100 yr for the four model simulations.

Models	PP_a^{50}	PP_a^{65}	Ψ_a^{30S}	Ψ_a^{0}	$\Psi_a^{26.5N}$	Ψ_a^{65N}
GFDL	−0.056	−0.057	−0.029	−0.040	−0.076	−0.013
CCCMA	−0.035	−0.033	−0.016	−0.026	−0.055	−0.038
MIROC	−0.046	−0.031	−0.024	−0.026	−0.042	−0.043
NCAR	−0.043	−0.035	−0.031	−0.044	−0.058	−0.024

deeper in the actual overturning than in the push–pull modes (Fig. 12). In contrast to the equatorial MOCs, the models do not agree on the magnitude of the difference between $\Psi_a^{26.5N}$ and the push–pull mode. In particular, PP_a^{65} (PP_a^{50}) is close to $\Psi_a^{26.5N}$ in MIROC (NCAR) simulations but noticeably different in GFDL (Fig. 6) and CCCMA (Fig. 11).

The models agree well on the relative importance of various components of the push–pull mode. In all simulations, the heat flux component dominates over the freshwater component in the surface push–pull mode (not shown). Initially (years 2001–05), $1/2\Psi_a^{30S}$ exceeds the maximum in SPP_a^{65D} by 5%–7% (CCMA and GFDL) to 24%–30% (NCAR and MIROC). Interestingly, the relative importance of the lateral boundary contribution increases with time, and its ratio with the surface push–pull mode reaches 1.2 (GFDL and CCMA) and 2.9–3.4 (MIROC and NCAR). The latter fact is explained by a weaker (possibly delayed) response of Ψ_a^{30S} to atmospheric forcing (Table 4). Such a delay can be expected to amplify changes in the North Atlantic MOC (Kamenkovich and Radko 2011). The maxima in SPP_a^{65D} and Ψ_a^{30S} (not shown) are also found at nearly the same densities in all models except CCCMA, where the surface push–pull mode has a maximum at lighter densities.

6. Summary and conclusions

This study analyzes the response of the isopycnal MOC to atmospheric forcing in model simulations of the twenty-first century climate. A novel aspect of this study is the focus on the push–pull mode, the component of the MOC directly forced by the surface buoyancy fluxes and the lateral exchanges at the northern flank of the ACC and at the subpolar latitudes in the Northern Hemisphere. This boundary-forced circulation can, therefore, be regarded as an adiabatic mode of circulation below the mixed layer. The analysis of the push–pull mode allows investigation of the mechanisms that cause changes in the MOC, such as the surface buoyancy forcing and lateral exchanges with the Southern Ocean, and estimation of the relative importance of the semi-adiabatic dynamics in the MOC. The push–pull mode and the isopycnal overturning are calculated for climate

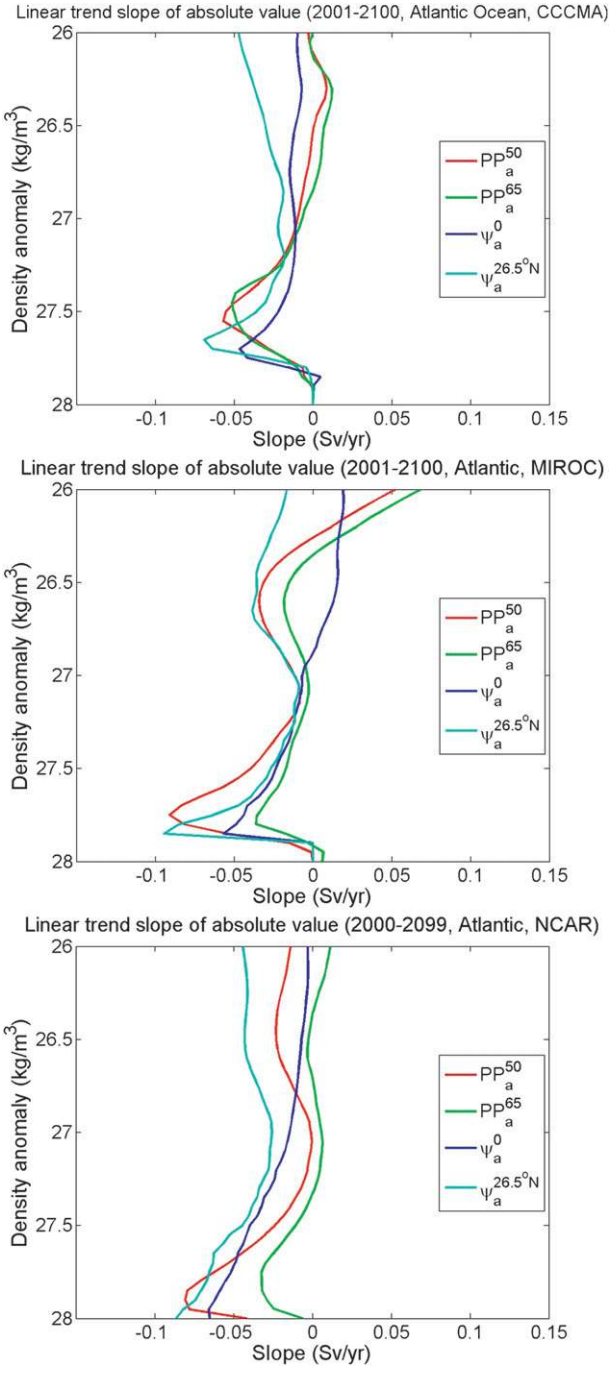

FIG. 12. Linear trends in the Atlantic MOC in three IPCC models: (top) CCCMA, (middle) MIROC, and (bottom) NCAR. The slopes of the linear trend are shown (Sv yr^{-1}) as functions of density for PP_a^{50} (red), PP_a^{65} (green), Ψ_a^{0} (blue), and $\Psi_a^{26.5N}$ (cyan).

simulations with four IPCC models; a detailed analysis is performed for one simulation only (GFDL CM2.1). The choice of this model was made on the basis of relatively accurate simulations of the Southern Ocean stratification and circulation (Russell et al. 2006; Sloyan and

Kamenkovich 2007). The push–pull mode is compared with the actual isopycnal overturning at two latitudes: at the equator (Ψ_a^0) and at 26.5°N ($\Psi_a^{26.5\mathrm{N}}$).

In the polar and subpolar North Atlantic, where the deep water forms, the density flux into the ocean is decreasing throughout the 100 years of all four simulations. As a result, the push–pull mode and the actual overturning both weaken, exhibiting a nearly linear downward trend in the magnitude of volume transport, accompanied by significant interannual variability. In the Atlantic, the maxima in PP_a^{65}, Ψ_a^0, and $\Psi_a^{26.5\mathrm{N}}$ decrease by 22%–34% and shift to lighter density during the 2001–2100 period. The overall agreement between the push–pull mode and actual isopycnal overturning strongly suggests a largely adiabatic, pole-to-pole response of the MOC to the global warming. In particular, PP_a and Ψ_a^0 in the GFDL model are very close to each other in the deep layers, and the differences between them are within approximately 10% of Ψ_a^0 in the layers below 27.55 kg m^{-3}. The decrease in the component of the push–pull mode that is due to surface fluxes significantly influences the reduction of the push–pull mode in the deep layers. The formulation of the push–pull mode allows explicit evaluation of the relative importance of the heat and freshwater fluxes in explaining weakening of the adiabatic MOC, and the analysis demonstrates the primary importance of the heat flux in all four models. Note that, strictly speaking, this does not imply that the freshwater fluxes play a minor role in weakening of the total MOC since they can influence surface heat/gain through changes in circulation. The contribution of the volume fluxes across 30°S is, however, even more substantial and tends to increase, in relative terms, throughout the 2001–2100 period. The latter fact is explained by a weaker decrease in the circulation at 30°S, in comparison to the North Atlantic.

Some differences between the push–pull mode and actual MOC are, however, noticeable. They are attributed primarily to the presence of internal processes, such as diapycnal fluxes and isopycnal volume drifts, not taken into account in the formulation of the push–pull mode. In this regard, the spatial distribution of these internal processes is the key factor. In particular, the push–pull mode is expected to most closely match the actual isopycnal MOC at the latitude around which the distribution of these processes is nearly symmetric [see appendix and Eqs. (A6) and (A7)]. The interhemispheric asymmetry in the MOC response to the atmospheric forcing is thus the key factor controlling the differences between the equatorial MOC and push–pull mode. It is noteworthy, however, that biases in simulation of diapycnal processes in these models are still uncertain and may be very significant.

The ability of the push–pull mode to capture a portion of the temporal variability in the actual MOC suggests both the importance of adiabatic mechanisms and the efficiency of cross-basin signal communication. The closest agreement between the push–pull mode and actual MOC is observed in the linear trends in the deep ocean. Consistent with this result, the correlation between decadal anomalies in PP_a and Ψ_a^0 is also very strong and exceeds 0.8 for a wide range of densities, especially for those heavier than 27.4 kg m^{-3}. This result suggests that the semiadiabatic push–pull mode captures a large portion of the interdecadal variability of the actual MOC, and, in turn, points to largely adiabatic mechanisms of these changes. At the interannual time scales, the correlation is substantially weaker but still exceeds 0.4 at several values of the time lag. The above correlations, particularly those of decadal anomalies, indicate the importance of the interplay between several processes linking the high and low latitudes, including a fast mechanism governed by Kelvin waves and slow mechanisms involving Rossby waves and advection within deep western boundary currents. The effectiveness of this cross-basin connection is intriguing, given the expected difficulty of intrahemispheric connections (Kawase 1987; Johnson and Marshall 2004).

Evolution of the MOC in the Indo-Pacific basin is more complicated than in the Atlantic, and one can expect a reduced importance of the push–pull mechanism in the Indo-Pacific basin (Radko et al. 2008). The changes in the global push–pull mode (PP_w) and the actual isopycnal MOC (Ψ_w) are, nevertheless, both shown to be similar in the GFDL model. In particular, the changes in the maximum PP_w^{65} and Ψ_w^0, corresponding densities, and linear trends are very similar.

The push–pull modes and actual isopycnal MOC are also analyzed for CCCMA, MIROC, and NCAR simulations. The analysis of these very different simulations helps to assess the robustness of the main conclusions of this study. The differences in Ψ_a^0 between these simulations are substantial, but the maximum transports in the actual equatorial MOC are close to at least one of the push–pull modes (PP_a^{65} or PP_a^{50}) in all simulations. The downward linear trend in Ψ_a^0 is generally consistent with the push–pull mode, although some differences are noticeable. In all simulations, the heat flux component dominates over the freshwater component in the surface push–pull mode.

To summarize the above, we find that the changes in the push–pull mode and the actual overturning are consistent in the deep layers, which suggests a direct link between changes in the surface forcing and lateral exchanges at the northern flank of ACC and the actual isopycnal MOC. These results emphasize the importance of the semiadiabatic, pole-to-pole push–pull mechanism

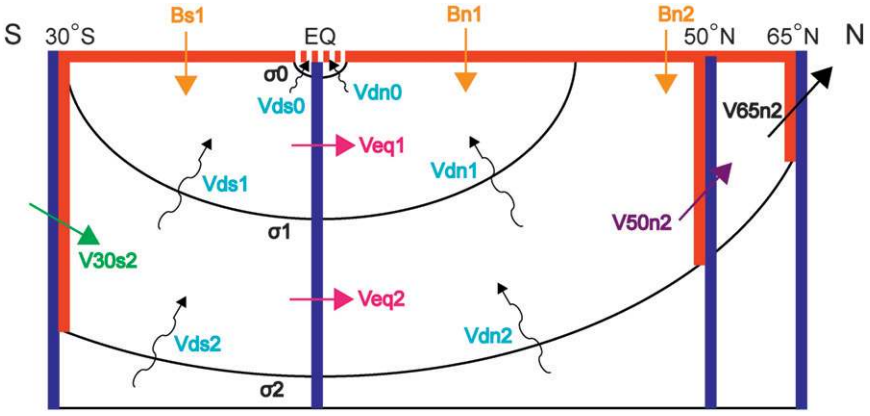

FIG. A1. Illustration of the isopycnal volume balance in two density layers.

in MOC variability. It also opens a possibility of the interpretation of the GCM-simulated MOC projections using overturning in the Southern Ocean and surface buoyancy forcing. There are, however, some noticeable differences between the push–pull mode and the actual isopycnal MOC, related primarily to the spatial distribution of transformations inside an oceanic basin. Analysis of model simulations has clear advantages, since all fields are known exactly. Ideally, a study like this one should be extended to the analysis based on the observed surface fluxes, stratification, and MOCs, such as those measured by the Rapid Climate Change–Meridional Overturning Circulation and Heatflux Array (RAPID–MOCHA; Cunningham et al. 2007). However, large uncertainties in these fields make such analyses unfeasible at the present time and likely into in the near future.

Acknowledgments. M.H. and I.K. acknowledge the support by the National Science Foundation, Grant OCE 0749723; T.R. acknowledges the support by NSF Grant OCE 0623524. Comments from three anonymous reviewers helped to improve this manuscript a great deal.

APPENDIX

Push–Pull Mode in Two Isopycnal Layers

The procedure for calculating the push–pull mode is illustrated here on the example of two isopycnal layers (Fig. A1). Note that the layers are assumed to be infinitely thin and thus exaggerated in the figure. Terms $B_{s1,2}$ and $B_{n1,2}$ stand for the volume transport from the mixed layer into layers 1 and 2, given by

$$B_{s,n1} = B_{s,n}(\sigma_1) - B_{s,n}(\sigma_0) \quad \text{and}$$
$$B_{s,n2} = B_{s,n}(\sigma_2) - B_{s,n}(\sigma_1). \tag{A1}$$

$V_{\text{eq}1,2}$, $V_{30s1,2}$, and V_{65n2} stand for the meridional volume flux inside layers 1 and 2; $V_{ds1,2}$ and $V_{dn1,2}$ are the diapycnal fluxes across the isopycnal surfaces 1 and 2. In the Southern Hemisphere (from 30°S to the equator), the divergence of the volume flux $dV_{s1,2}$ is given by

$$B_{s1} + V_{30s1} + V_{ds1} - V_{ds0} - V_{\text{eq}1} = dV_{s1}, \tag{A2}$$

$$V_{30s2} - V_{ds1} + V_{ds2} - V_{\text{eq}2} = dV_{s2}. \tag{A3}$$

Note that only one layer outcrops in this region. Similarly, we can write the following expressions in the Northern Hemisphere (from the equator to 65°N):

$$B_{n1} + V_{\text{eq}1} + V_{dn1} - V_{dn0} = dV_{n1}, \tag{A4}$$

$$V_{\text{eq}2} + V_{dn2} - V_{dn1} + B_{n2} - V_{65n2} = dV_{n2}. \tag{A5}$$

Subtraction of (A2) and (A3) from (A4) and (A5) leads to the expressions of the cross-equatorial transports in each layer:

$$\begin{aligned} V_{\text{eq}1} = {} & \frac{1}{2}(B_{s1} - B_{n1}) + \frac{1}{2}(V_{dn0} - V_{dn1} - V_{ds0} + V_{ds1}) \\ & + \frac{1}{2}V_{30s1} + \frac{1}{2}(dV_{n1} - dV_{s1}) = V_{pp1}(\sigma) \\ & + \frac{1}{2}(V_{dn0} - V_{dn1} - V_{ds0} + V_{ds1}) + \frac{1}{2}(dV_{n1} - dV_{s1}), \end{aligned} \tag{A6}$$

$$\begin{aligned} V_{\text{eq}2} = {} & \frac{1}{2}(B_{s2} - B_{n2}) + \frac{1}{2}(V_{dn1} - V_{dn2} - V_{ds1} + V_{ds2}) \\ & + \frac{1}{2}(V_{30s2} + V_{65n2}) + \frac{1}{2}(dV_{n1} - dV_{s1}) = V_{\text{pp}2}(\sigma) \\ & + \frac{1}{2}(V_{dn1} - V_{dn2} - V_{ds1} + V_{ds2}) + \frac{1}{2}(dV_{n1} - dV_{s1}). \end{aligned} \tag{A7}$$

The terms V_{ppn} stand for the push–pull mode, and their difference with V_{eqn} is then due to the net contribution of the cross-isopycnal volume transport [second bracketed terms in (A6) and (A7)] and the isopycnal volume drifts (third bracketed terms on the right-hand side). Note that if the distribution of these transformations is purely symmetric around the equator, the push–pull modes will be exactly equal to the actual isopycnal volume fluxes.

REFERENCES

Boccaletti, G., R. Ferrari, A. Adcroft, D. Ferreira, and J. Marchall, 2005: The vertical structure of ocean heat transport. *Geophys. Res. Lett.,* **32,** L10603, doi:10.1029/2005GL022474.

Bryan, F., 1987: Parameter sensitivity of primitive equation ocean general circulation models. *J. Phys. Oceanogr.,* **17,** 970–985.

Clark, P. U., N. G. Pisias, T. F. Stocker, and A. J. Weaver, 2002: The role of the thermohaline circulation in abrupt climate change. *Nature,* **415,** 863–869.

Cunningham, S., and Coauthors, 2007: Temporal variability of the Atlantic meridional overturning circulation at 26.5°N. *Science,* **317,** 935–938.

DDC IPCC, cited 2010: The SRES emissions scenarios. [Available online at http://sedac.ciesin.columbia.edu/ddc/sres/.]

Dixon, K. W., T. L. Delworth, M. J. Spelman, and R. J. Stouffer, 1999: The influence of transient surface fluxes on North Atlantic overturning in a coupled GCM climate change experiment. *Geophys. Res. Lett.,* **26,** 2749–2752.

Donners, J., S. S. Drijfhout, and W. Hazeleger, 2005: Water mass transformation and subduction in the South Atlantic. *J. Phys. Oceanogr.,* **35,** 1841–1860.

Downes, S. M., A. Gnanadesikan, S. M. Griffies, and J. L. Sarmiento, 2011: Water mass exchange in the Southern Ocean in coupled climate models. *J. Phys. Oceanogr.,* **41,** 1756–1771.

Flato, G. M., G. J. Boer, W. G. Lee, N. A. McFarlane, D. Ramsden, M. C. Reader, and A. J. Weaver, 2000: The Canadian Centre for Climate Modelling and Analysis global coupled model and its climate. *Climate Dyn.,* **16,** 451–467.

Gnanadesikan, A., 1999: A simple predictive model for the structure of the oceanic pycnocline. *Science,* **283,** 2077–2079.

Goodman, P., 2001: Thermohaline adjustment and advection in an OGCM. *J. Phys. Oceanogr.,* **31,** 1477–1497.

Gregory, J. M., and Coauthors, 2005: A model intercomparison of changes in the Atlantic thermohaline circulation in response to increasing atmospheric CO_2 concentration. *Geophys. Res. Lett.,* **32,** L12703, doi:10.1029/2005GL023209.

Griffies, S. M., and Coauthors, 2005: Formulation of an ocean model for global climate simulations. *Ocean Sci.,* **1,** 45–79.

Grist, J. P., R. Marsh, and S. A. Josey, 2009: On the relationship between the North Atlantic meridional overturning circulation and the surface-forced overturning streamfunction. *J. Climate,* **22,** 4989–5002.

Han, M., 2011: A study on the relationship between the air–sea density flux and isopycnal meridional overturning circulation in a warming climate. M.S. thesis, Meteorology and Physical Oceanography, University of Miami, 253 pp.

Hasumi, H., and S. Emori, 2004: K-1 coupled GCM (MIROC) description, K-1 Tech. Rep. 1, 34 pp. [Available online at http://www.ccsr.u-tokyo.ac.jp/kyosei/hasumi/MIROC/tech-repo.pdf.]

Ivchenko, V. O., V. B. Zalesny, and M. R. Drinkwater, 2004: Can the equatorial ocean quickly respond to Antarctic sea ice/salinity anomalies? *Geophys. Res. Lett.,* **31,** L15310, doi:10.1029/2004GL020472.

Johnson, H. L., and D. P. Marshall, 2004: Global teleconnections of meridional overturning circulation anomalies. *J. Phys. Oceanogr.,* **34,** 1702–1722.

Kamenkovich, I., and T. Radko, 2011: Role of the Southern Ocean in setting the Atlantic stratification and meridional overturning circulation. *J. Mar. Res.,* **69,** 277–308.

——, A. Sokolov, and P. H. Stone, 2003: Feedbacks affecting the response of the thermohaline circulation to increasing CO_2: A study with a model of intermediate complexity. *Climate Dyn.,* **21,** 119–130.

Kawase, M., 1987: Establishment of deep ocean circulation driven by deep-water production. *J. Phys. Oceanogr.,* **17,** 2294–2317.

Klinger, B. A., and J. Marotzke, 1999: Behavior of double-hemisphere thermohaline flows in a single basin. *J. Phys. Oceanogr.,* **29,** 382–399.

Latif, M., E. Roeckner, U. Mikolajewicz, and R. Voss, 2000: Tropical stabilization of the thermohaline circulation in a greenhouse warming simulation. *J. Climate,* **13,** 1809–1813.

Ledwell, J. R., A. J. Watson, and C. S. Law, 1993: Evidence for slow mixing across the pycnocline from an open-ocean tracer-release experiment. *Nature,* **364,** 701–703.

Mahajan, S., R. Zhang, and T. L. Delworth, 2011: Impact of the Atlantic Meridional Overturning Circulation (AMOC) on Arctic surface air temperature and sea ice variability. *J. Climate,* **24,** 6573–6581.

Manabe, S., and R. J. Stouffer, 1994: Multiple century response of a coupled ocean–atmosphere model to an increase of atmospheric carbon dioxide. *J. Climate,* **7,** 5–23.

Marotzke, J., and J. R. Scott, 1999: Convective mixing and the thermohaline circulation. *J. Phys. Oceanogr.,* **29,** 2962–2970.

——, and B. A. Klinger, 2000: Dynamics of equatorially asymmetric thermohaline circulations. *J. Phys. Oceanogr.,* **30,** 955–970.

Marshall, J., D. Jamous, and J. Nilsson, 1999: Reconciling thermodynamic and dynamic methods of computation of water-mass transformation rates. *Deep-Sea Res. I,* **46,** 545–572.

Meehl, G. A., and Coauthors, 2007: Global climate projections. *Climate Change 2007: The Physical Science Basis,* S. Solomon et al., Eds., Cambridge University Press, 747–845.

Mikolajewicz, U., and R. Voss, 2000: The role of the individual air–sea flux components in CO_2-induced changes of the ocean's circulation and climate. *Climate Dyn.,* **16,** 627–642.

Radko, T., 2007: A mechanism for establishment and maintenance of the meridional overturning in the upper ocean. *J. Mar. Res.,* **65,** 85–116.

——, and I. Kamenkovich, 2011: Semi-adiabatic model of the deep stratification and meridional overturning. *J. Phys. Oceanogr.,* **41,** 751–780.

——, ——, and P.-Y. Dare, 2008: Inferring the pattern of the oceanic meridional transport from the air–sea density flux. *J. Phys. Oceanogr.,* **38,** 2722–2738.

Russell, J. L., R. J. Souffer, and K. W. Dixon, 2006: Intercomparison of the Southern Ocean circulations in the IPCC coupled model control simulations. *J. Climate,* **19,** 4560–4575.

Samelson, R. M., 2004: Simple mechanistic models of middepth meridional overturning. *J. Phys. Oceanogr.,* **34,** 2096–2103.

——, 2009: A simple dynamical model of the warm-water branch of the mid-depth meridional overturning cell. *J. Phys. Oceanogr.,* **39,** 1216–1230.

Schmitt, R. W., P. S. Bogden, and C. E. Dorman, 1989: Evaporation minus precipitation and density fluxes for the North Atlantic. *J. Phys. Oceanogr.,* **19,** 1208–1221.

Schmittner, A., and T. F. Stocker, 1999: The stability of the thermohaline circulation in global warming experiments. *J. Climate,* **12,** 1117–1133.

Sévellec, F., and A. V. Fedorov, 2011: Stability of the Atlantic meridional overturning circulation and stratification in a zonally-averaged ocean model: Effects of freshwater flux, Southern Ocean winds, and diapycnal diffusion. *Deep-Sea Res. II,* **58,** 1927–1943.

Sloyan, B. M., and I. V. Kamenkovich, 2007: Simulation of Subantarctic Mode and Antarctic Intermediate Waters in climate models. *J. Climate,* **20,** 5061–5080.

Smith, R., and P. Gent, Eds., 2004: Reference manual for the Parallel Ocean Program (POP): Ocean component of the Community Climate System Model (CCSM2.0 and 3.0). Rep. LAUR-02-2484, 75 pp. [Available online at http://www.cesm.ucar.edu/models/ccsm3.0/pop/doc/manual.pdf.]

Speer, K., and E. Tziperman, 1992: Rates of water mass formation in the North Atlantic Ocean. *J. Phys. Oceanogr.,* **22,** 93–104.

——, H.-J. Isemer, and A. Biastoch, 1995: Water mass formation from revised COADS data. *J. Phys. Oceanogr.,* **25,** 2444–2457.

Stouffer, R. J., and Coauthors, 2006: Investigating the causes of the response of the thermohaline circulation to past and future climate changes. *J. Climate,* **19,** 1365–1387.

Talley, L. D., J. L. Reid, and P. E. Robbins, 2003: Notes and correspondence: Data-based meridional overturning streamfunction for the global ocean. *J. Climate,* **16,** 3213–3226.

Tandon, A., and K. Zahariev, 2001: Quantifying the role of mixed layer entrainment for water mass transformation in the North Atlantic. *J. Phys. Oceanogr.,* **31,** 1120–1131.

Toggweiler, J. R., and B. Samuels, 1998: On the ocean's large scale circulation near the limit of no vertical mixing. *J. Phys. Oceanogr.,* **28,** 1832–1852.

Toole, J., K. Polzin, and R. Schmitt, 1994: Estimates of diapycnal mixing in the abyssal ocean. *Science,* **264,** 1120–1123.

Walin, G., 1982: On the relation between sea-surface heat flow and thermal circulation in the ocean. *Tellus,* **34,** 187–195.

Wiebe, E. C., and A. J. Weaver, 1999: On the sensitivity of global warming experiments to the parameterisation of sub-grid scale ocean mixing. *Climate Dyn.,* **15,** 875–893.

Wolfe, C. L., and P. Cessi, 2010: What sets the strength of the middepth stratification and overturning circulation in eddying ocean models? *J. Phys. Oceanogr.,* **40,** 1520–1538.

Zhang, R., 2008: Coherent surface-subsurface fingerprint of the Atlantic meridional overturning circulation. *Geophys. Res. Lett.,* **35,** L20705, doi:10.1029/2008GL035463.